THE ASTROPHYSICAL JOURNAL, 451:758–767, 1995 October 1


# SILICATE EMISSION AT 10 MICRONS IN VARIABLES ON THE ASYMPTOTIC GIANT BRANCH

G. C. SLOAN[1] AND S. D. PRICE
Geophysics Directorate, Phillips Laboratory, PL/GPOB, 29 Randolph Road, Hanscom AFB, MA 01731-3010;
sloan@ssa1.arc.nasa.gov, price@pldac.plh.af.mil
*Received 1994 May 24; accepted 1995 April 12*

## ABSTRACT

We show that the observed shapes of the silicate emission profile at 10 $\mu$m are described by a sequence from the classic, narrow silicate emission feature peaking at 10 $\mu$m to a broad, low-contrast feature which peaks longward of 11 $\mu$m. We use this silicate dust sequence as the basis for a new system to classify the silicate emission feature, apply it to spectra taken by the *IRAS* Low-Resolution Spectrometer (LRS) for a flux-limited sample of variable stars on the asymptotic giant branch (AGB), and compare our system to previous classification systems of the LRS spectra. Our results suggest that either AGB stars produce multiple shells during their evolution or that spectra from oxygen-rich dust shells do not evolve from broad to narrow emission.

*Subject headings:* circumstellar matter — infrared: stars — stars: AGB and post-AGB

## 1. INTRODUCTION

The *Infrared Astronomical Satellite* (*IRAS*), which took data from 1983 January to November, fundamentally changed the field of infrared astronomy. Its Low-Resolution Spectrometer (LRS) obtained by far the largest collection of infrared spectra taken with one instrument. One of the strongest and most common features in these spectra is the well-known 10 $\mu$m emission attributed to silicate dust. The wide variety of widths, contrasts, and shapes of this feature in the LRS database, discussed by Little-Marenin & Price (1986), proved surprising. Little-Marenin & Little (1988, 1990) continued this study by developing a classification system for the various spectra (hereafter LML classification). Their different classes probably represent different oxygen-rich dust chemistries and may in fact depict stages in the development of dust shells around evolved stars (Stencel et al. 1990).

We wish to develop a less subjective version of the LML classification system in order to improve our understanding of how stars known to be in their final evolutionary stages shed their envelopes before becoming planetary nebulae. We concentrate on the classes of long-period variables known to be on the asymptotic giant branch (AGB), namely, Mira variables, semiregular variables of classes SRa and SRb, and irregular variables of class Lb. We also compare and interpret our classification system with respect to the LML system and two other systems, the LRS characterizations (*IRAS* Science Team 1986, hereafter LRS Atlas; Beichman et al. 1988) and the autoclasses described by Cheeseman et al. (1989) and Goebel et al. (1989).

### 1.1. *Low-Resolution Spectrometer Characterizations*

The first system used to classify the wide range of spectra obtained by the LRS was the set of LRS characterizations that accompanied the initial release of the *IRAS* data (LRS Atlas). This system was developed as a means of quickly labeling the most significant characteristics of the spectra. Each spectrum is designated with a two-digit number. The first digit gives the basic shape of the spectrum, while the second quantifies the dominant feature in the spectrum. Most late-type stars with silicate or related emission fall into the 2*n* group (i.e., 21–29), though a large minority are characterized as 1*n* (mostly 14–17), and a few are classed as 02.

The 1*n* group represents blue spectra with no recognized features stronger than 5 times the rms noise or 10% of the continuum. For these spectra, the second digit is the spectral index; $n = -2\beta$, where $\beta$ is defined by fitting $F_\lambda \propto \lambda^\beta$ between 8 and 13 $\mu$m. A spectrum characterized as 18 has no excess emission, and its flux drops off more steeply with wavelength than a spectrum of characterization 15.

The 2*n* group are blue spectra with silicate emission at 9.8 $\mu$m. The second digit denotes the silicate emission strength: $n = 10B_{9.8\mu m}$, where $B_{9.8\mu m}$ is the band strength. In general, the band strength depends on the ratio of the actual flux to the estimated continuum flux: $B_\lambda = \ln(F_\lambda/F_{\lambda c})$. For emission at 9.8 $\mu$m, the continuum is defined as

$$\ln(F_{\lambda c}) = 0.589 \ln(F_{7.9\mu m}) - 0.411 \ln(F_{13.3\mu m}) .$$

This definition is only valid if the dust does not contribute to the spectrum at 7.9 or 13.3 $\mu$m, but it is now known that silicate dust does show substantial emission between the two prominent features at 10 and 20 $\mu$m (e.g., Draine & Lee 1984; Ossenkopf, Henning, & Mathis 1992).

### 1.2. *Autoclasses*

The AutoClass II Program used a Bayesian approach to divide the LRS database into a series of self-consistent classes instead of basing its classification on a priori parameters. It grouped all of the spectra in the LRS Atlas into 70 different classes, which were then organized into nine meta-classes. The majority of spectra considered in this paper fall into one of three meta-classes, $\beta$0–13, the silicate emission classes, $\delta$0–8, relatively featureless spectra, and $\lambda$0–35, a group of weak-featured spectra of intermediate temperatures. Only a few of

[1] Postal address: NASA/Ames Research Center, MS 245-6, Moffett Field, CA 94035-1000.

the 70 classes are significantly populated by our sample of AGB variables.

### 1.3. *LML Classification*

Little-Marenin and Little limited their classification to silicates and related oxygen-rich dust. Their approach was unique in that, rather than trying to classify the entire spectrum, they focused on the dust emission after removing the stellar contribution. This effectively eliminated the influence of the shell contrast on the classification process. It also led to the neat grouping of nearly all of the many emission profiles studied into six distinct classes.

The LML classification is a sequence from the classic, narrow emission feature at 10 $\mu$m (classed as Silicate) to features with progressively stronger contributions at 11 $\mu$m (Silicate+ and Silicate++) to broad, low-contrast emission peaking longward of 11 $\mu$m (Broad). They defined two additional classes: a 3-component class, similar to Silicate++ but possessing an additional emission feature at 13 $\mu$m, and an S class, which contained a silicate-like feature peaking around 10.5–10.8 $\mu$m rather than at 9.7 $\mu$m.

To remove the continuum contribution, Little-Marenin & Little (1988) originally used the blackbody that matched the 8 and 14 $\mu$m spectral fluxes. In some cases this method resulted in continuum temperatures as low as 600 K, too low to represent just the stellar continuum. Because dust emission can contribute at 14 $\mu$m, this method removes some of the dust emission from the final spectrum. Subsequently, Little-Marenin & Little (1990) used a 2500 K Planck function scaled to the continuum at 8 $\mu$m for all stars. This avoids the problem at 14 $\mu$m and makes the reasonable assumption that the silicate emission is negligible at 8 $\mu$m. The assumption that the photosphere of all late-type stars showing dust emission can be modeled with a single Planck function may be called into question, but as we will show below, it introduces only small systematic effects which should not influence the classification scheme.

## 2. DEFINING A NEW CLASSIFICATION SYSTEM

### 2.1. *The Sample of Variable Giants*

Our goal was to obtain an infrared flux-limited sample of AGB variable stars with silicate emission. We concentrated on the four classes of variables associated with the AGB: Mira, SRa and SRb (semiregular), and Lb (irregular) (Hoffmeister, Richter, & Wenzel 1984). We excluded SRc and Lc variables, as these are associated with supergiants, and SRd variables because they are usually associated with spectral classes of F, G, and K and are probably not AGB stars. We extracted a list of these variables from Kholopov et al. (1985–1988, hereafter GCVS), and cross-referenced it with the *IRAS* Point Source Catalog (1988), hereafter PSC. We used the catalogs distributed by the NASA Astronomical Data Center on CD-ROM.

We limited our sample to sources brighter than 28 Jy at 12 $\mu$m to exclude sources with noisy LRS data. We further limited our sample to only those sources with confirmed normal oxygen-rich optical spectra in the GCVS or SIMBAD database. We adopt as oxygen-rich those stars with spectral classes K, M, and MS, as well as S stars with abundance indices of 1 or 2. Table 1 illustrates the steps used to define our sample and the results.

The PSC is complete at a 12 $\mu$m flux limit of 28 Jy except for the 4% of the sky not covered; the primary limit to our completeness comes from the GCVS. Hoffmeister et al. (1984) estimate that only a small fraction of the irregular variables have been recognized. Most of these missing stars, though, have very low amplitudes of variability (like $\alpha$ Tau) and have probably not begun to lose conspicuous amounts of mass. The fraction of missing semiregulars is smaller. Finally, Hoffmeister et al. (1984) claim that all Mira variables with maximum visual magnitudes brighter than 11 have been detected. For optically thin shells, this limit is well within our flux limit at 12 $\mu$m. The GCVS selects against heavily enshrouded Mira variables too faint to be identified visually, but most of these sources will show dust absorption at 10 $\mu$m and should not be a part of our sample of silicate emission sources.

TABLE 1

THE SAMPLE OF VARIABLES ON THE ASYMPTOTIC GIANT BRANCH

| SET | VARIABILITY CLASS | | | | TOTAL |
|---|---|---|---|---|---|
| | Mira | SRa | SRb | Lb | |
| GCVS | 5822 | 845 | 896 | 1606 | 9169 |
| In PSC, [12] < 0 | 302 | 40 | 194 | 147 | 683 |
| Bright sources in PSC: | | | | | |
| O-rich | 241 | 29 | 157 | 119 | 546 |
| S star | 11 | 1 | 4 | 2 | 18 |
| C star | 33 | 9 | 33 | 24 | 99 |
| No spectral class | 17 | 1 | 0 | 2 | 20 |
| Bright O-rich sources in PSC: | | | | | |
| Silicate emission | 232 | 28 | 126 | 67 | 453 |
| Silicate self-absorption | 3 | 0 | 0 | 0 | 3 |
| Naked star | 2 | 1 | 30 | 51 | 84 |
| Other | 4 | 0 | 1 | 1 | 6 |

We wish to exclude C and S stars because of their unusual chemistries (S stars with abundance indices of 1 or 2 are not excluded because the TiO bands are still stronger than the ZrO bands, indicating only weak deviations from normal oxygen-rich chemistry). Selecting only sources with known oxygen-rich optical spectra guarantees a purer sample. This criterion also excludes some of the oxygen-rich stars which have no optical spectral classification, but, as Table 1 illustrates, the number of such sources is small.

### 2.2. *Preparing a Spectrum*

We obtained a spectrum from the LRS database maintained at the University of Calgary for each of the sources in our sample of bright O-rich AGB variables. These spectra were published either in the LRS Atlas or by Volk & Cohen (1989). The LRS Atlas contains 5425 spectra, all an average of two or more individual scans, usually measured months apart. Volk & Cohen (1989) published an additional set of 356 LRS spectra not included in the LRS Atlas. Wildeman, Beintema, & Wesselius (1983) and Beichman et al. (1988) discuss the instrument and methods of data acquisition and reduction.

Data from the two separate sets of detectors, one covering 7.67–13.55 $\mu$m (the blue spectrum) and the other covering 11.37–22.92 $\mu$m (the red spectrum), are combined to produce a single LRS spectrum. We spliced the spectra together so that the last wavelength element in the blue portion falls at 13.34 $\mu$m and the first red element falls at 13.41 $\mu$m in order to preserve good resolution over the 13 $\mu$m feature seen in some spectra.

### 2.3. *Separating the Stellar Continuum from the Dust Emission*

The LRS database was originally calibrated using the spectrum of $\alpha$ Tau as a standard under the assumption that it

could be characterized as a perfect $10^4$ K blackbody. This procedure distorts the LRS spectra in two ways. Cohen, Walker, & Witteborn (1992) have shown that $\alpha$ Tau in fact has significant SiO absorption at 8 $\mu$m (11% of the stellar continuum at 8.0 $\mu$m at the LRS resolution). Also, Engelke (1992) found that the underlying photosphere of late-type stars does not emit as a blackbody with a single temperature. Cohen et al. (1992) have developed a set of factors which corrects each spectrum in the LRS database for these calibration problems. We apply these factors to each spectrum in our sample, producing what we will refer to as corrected LRS spectra.

To isolate the emission of the dust, we model the stellar continuum, fit it to the LRS data, and subtract it. To improve on the continuum used by LML (a 2500 K Planck function), we use an Engelke function with superposed SiO absorption. Because the LRS are time-averaged spectra, it is very difficult to assign a precise stellar temperature. (In the extreme case, the spectral class of some Mira variables can change from M5 to M10.) Had we chosen to use individual LRS scans, we might have been able to determine the temperature from the phase of the central star, but the lower signal-to-noise ratios of the individual scans would have forced us to reduce our sample size. These difficulties led us to assume a common temperature for our entire sample, just as done by LML. The average spectral class of our sample is approximately M6, corresponding to an effective temperature of 3240 K (Lang 1992; Engelke 1992).

The Engelke function (Engelke 1992) is a modified Planck function which allows the brightness temperature to decrease with wavelength:

$$B_\nu = B_\nu(T_b) ,$$

where

$$T_b = 0.738 T_{\rm eff}(1 + 79450/\lambda T_{\rm eff})^{0.182} ,$$

with $\lambda$ in microns and T in kelvins. This empirical relation models the effect of the $H^-$ ion, the dominant source of opacity in the mid-infrared. Its opacity increases with wavelength, resulting in a progressively cooler photosphere at longer wavelengths. The Engelke function provides a good match to computer models and observations of the infrared solar energy distribution; it can also be used to accurately model the spectral energy distribution of infrared standards (Engelke 1992; Cohen et al. 1992).

We model the SiO band by taking the median absorption profile in the corrected LRS spectra of five bright naked giants ($\alpha$ Tau, $\beta$ Peg, $\rho$ Per, V806 Cen, and NU Pav). The maximum absorption at 8 $\mu$m increases from 9% at K5 to 15% at M6 (at higher resolutions than the LRS, the maximum absorption depth would be greater). Rinsland & Wing (1982) investigated the first overtone of SiO at 4 $\mu$m and found a similar dependence of absorption with effective temperature. We could not investigate the behavior of the SiO absorption band beyond spectral class M6 because almost all later type stars in our sample contain excess dust emission which hides the photosphere.

Figure 1 illustrates our model stellar continuum, a 3240 K Engelke function with 15% SiO absorption. This continuum was scaled to each LRS spectrum by minimizing the $\chi^2$ difference over the wavelength range 7.67–8.58 $\mu$m. For most of our sample, the dust emission at these wavelengths is negligible. For some of the highest contrast shells, the dust contribution is noticeable at wavelengths as short as 8.0 $\mu$m, causing us to overestimate the photospheric contribution slightly. This error (which we estimate to be less than 5%) has no substantial effect on our classification method.

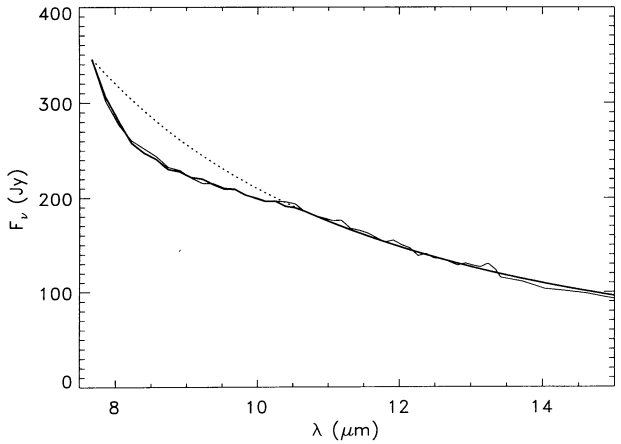


FIG. 1.—Our standard model for the stellar continuum from an M6 star (*thick line*), assumed to apply to all stars in our sample. The model is an Engelke function with an effective temperature of 3240 K with SiO absorption removed. The maximum SiO absorption is 15% at 8.2 $\mu$m. The dashed line shows how the Engelke function behaves in the absence of any SiO absorption. The corrected LRS spectrum of NU Pav, an M6 star with no excess emission, appears as a solid thin line.

While we have tried to depict the spectrum from the stellar photosphere as accurately as possible, we emphasize that the classifications are fairly insensitive to the specific nature of the assumed temperature of the stellar contribution. We performed a sensitivity analysis by varying the effective temperature of the stellar continuum by $\pm 400$ K. This temperature range covers the possible effective temperatures of nearly all Mira variables at all phases and introduces systematic errors smaller than the errors produced by the noise in the spectra for all but the brightest 15 or so stars. We also tested for the effect of the SiO absorption by excluding it from our continuum model. Again, this resulted in systematic errors smaller than the random errors in most of the spectra.

However, for the spectra with low-contrast contributions from the dust shell, uncertainty in the amount of SiO absorption may produce more significant errors. As explained above, it is difficult to estimate the depth of the SiO absorption in the coolest stars in our sample. The minimum SiO absorption in our sample would be about 10%; we believe the maximum to be on the order of 20%. For a dust emission contrast (defined in § 2.5) as small as 10%, deviations from our assumed 15% SiO depth could account for half the flux from the dust shell. Fortunately, nearly all of the spectra with silicate emission in our sample have dust emission contrasts greater than 10%; most have contrasts greater than 20%.

### 2.4. *Classification Procedure*

Once we have isolated the dust emission by removing the stellar contribution to the spectrum, we can classify the resulting spectrum. Most of the spectra in our sample contained silicate or related dust emission of some type. The majority of the sources without silicate emission contained no excess at all. A small fraction either had SiC emission (at 11.3 $\mu$m; possibly incorrect associations), were too noisy to characterize, or appeared very red, probably due to chance super-

position with an H II region. All of these were rejected from further consideration. In addition, three of the reddest sources in our sample based on [12]–[25] colors contained self-absorbed silicate emission and were also removed from the sample. These rejections reduced our final list to 537 sources, as summarized in Table 1.

An initial examination of the spectra with strong 13 $\mu$m emission revealed that the feature was not restricted to just the 3-component class, as suggested by the LML classifications. We were also unsure about the nature of their S class. However, the sequence of types Silicate–Silicate+–Silicate++ through Broad seemed clear. We base our classification method on this sequence from narrow to broad emission but depart from the LML system by treating the 13 $\mu$m emission feature separately and not using it as a distinguishing characteristic of any class.

To quantify the shape of the dust emission after removing the stellar contribution, we examined the fluxes at wavelengths of 10, 11, and 12 $\mu$m. The flux ratio $F_{10}/F_{11}$ gives an indication of the width of the 10 $\mu$m silicate emission feature, and the flux ratio $F_{10}/F_{12}$ provides information about the long-wavelength shoulder (all fluxes in this paper are treated in $F_\nu$ units). We found that these two flux ratios were tightly correlated, as illustrated in Figure 2. We can analytically represent this correlation with an empirical power law:

$$F_{10}/F_{12} = 1.32(F_{10}/F_{11})^{1.77} .$$

The flux ratios from all dust emission profiles in our sample fall on or near the curve defined by this power law. The distribution of points about the curve is statistically consistent with the hypothesis that all noise-free data would fall on or very close to the curve. Thus, we conclude that the empirical power law describes the shape of all observed emission profiles from oxygen-rich dust. Broad emission features lie to the lower left on the curve. Moving along the curve up and to the right, the dust emission profile grows progressively narrower, and the peak moves from longer wavelengths to 10 $\mu$m, resembling the classic silicate feature more and more closely.

Figures 2 and 5 clearly show that the broad emission feature, whatever its specific origin, is related in some way to the classic silicate feature. Consequently, we will refer to the curve in Figure 2 as the silicate dust sequence. For ease of reference, we will refer to a silicate emission index (defined below), which is based on the position of a spectrum along this sequence, even though the spectrum may arise from oxygen-rich dust of a related, but nonsilicate, chemistry.

We classify each dust emission spectrum in the following manner. The flux ratios $F_{10}/F_{11}$ and $F_{10}/F_{12}$ lie at a point in Figure 2 which usually does not fall right on the power-law curve. The position on the power-law curve closest to the actual data point (along a line orthogonal to the power-law curve) defines a pair of ratios $F_{10}/F_{11}$ and $F_{10}/F_{12}$, corrected for the noise, from which we determine a corrected flux ratio $F_{11}/F_{12}$. We define a silicate emission index.

$$n = 10(F_{11}/F_{12}) - 7.5 ,$$

which we use to classify the dust spectrum. The values of $n$ are truncated, not rounded. While the ratio $F_{11}/F_{12}$ covers a fairly large range of values (from 0.57 to 2.22), we limit the index to the range 1 to 8, so that sources with indices less than 1 are labeled as SE1 and indices greater than 8 as SE8. Figure 3 illustrates examples of dust emission profiles for each index.

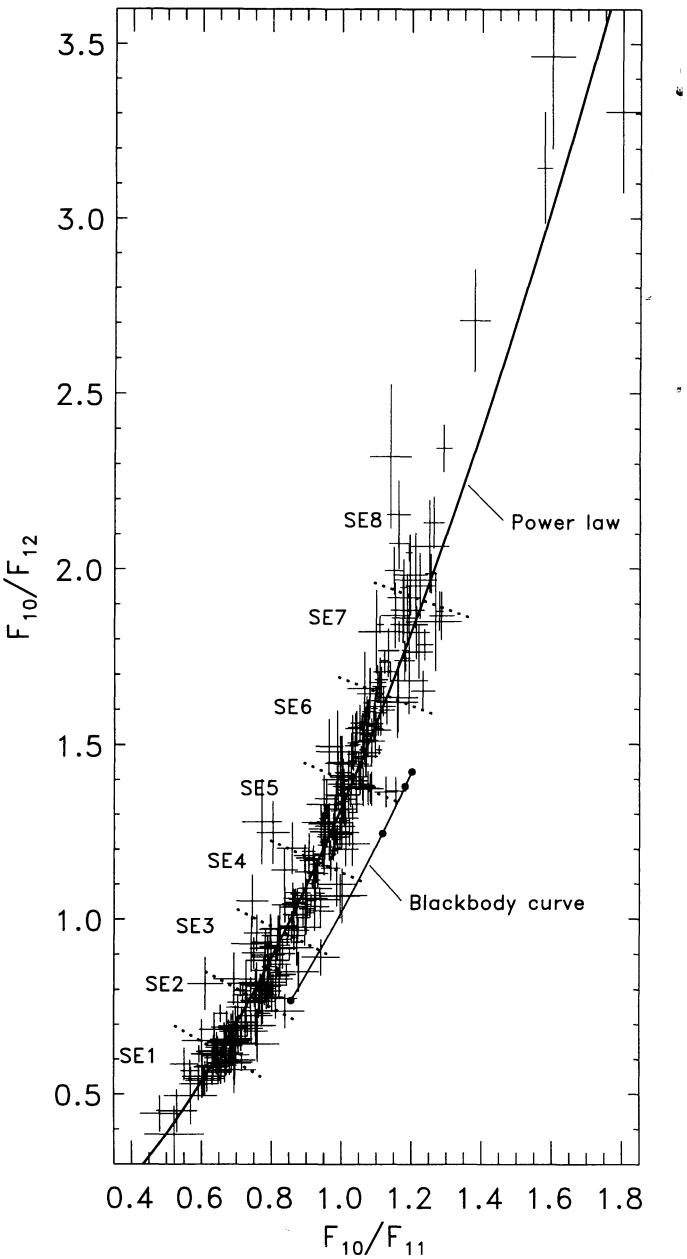


FIG. 2.—The silicate dust sequence. The flux ratio $F_{10}/F_{12}$ is plotted vs. $F_{10}/F_{11}$ for all sources with silicate emission of signal-to-noise ratio 10 or more. The error bars are either statistical 1 $\sigma$ errors or systematic errors (found by varying $T_{\rm eff}$ by $\pm 400$ K and the continuum fit by the uncertainty in the fit), whichever is larger (usually the statistical error). The thick solid line is the power-law fit, and the dashed lines are boundaries between silicate emission indices (see § 2.4). The points are for blackbodies of (from top to bottom) $10^4$ K, 3000 K, 1000 K, and 300 K.

The silicate emission index roughly follows the LML classifications: their Silicate class includes indices 6–8; the Broad class corresponds to indices 1–2.

### 2.5. *Dust Emission Contrast*

We also divide the total flux contained in the emission feature by the total flux under the stellar continuum over the wavelength range 7.67 to 14.03 $\mu$m. This ratio measures the contrast of the dust emission to the stellar continuum.

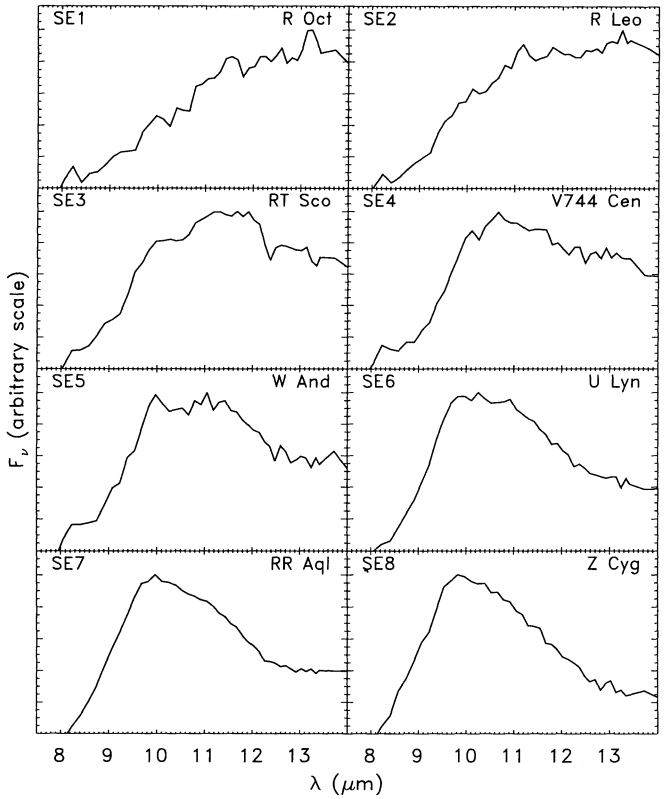


FIG. 3.—Sample spectra for each silicate emission index. The stellar contribution has already been removed from each spectrum, using the model stellar continuum illustrated in Fig. 1. Silicate Emission index 1 (SE1) represents the broadest profile observed, SE8 the narrowest. Generally, the contribution of the dust to the total spectrum for lower silicate emission indices is smaller.

Figure 4 illustrates the relationship between the dust emission contrast and the corrected flux ratio $F_{11}/F_{12}$. Broad emission profiles (lower $F_{11}/F_{12}$ ratios and lower silicate indices) are constrained to have low contrasts, but narrower emission profiles can have low or high contrasts. These results are best described as a limit to the possible contrast of a dust shell which increases as the emission profile grows narrower. While a few spectra are clearly above this limit, they can be explained as statistical fluctuations from noisy spectra.

### 2.6. *Equivalent Flux of the* 13 μm *Feature*

We estimate the flux from the 13 μm feature for each spectrum by fitting a polynomial to the dust continuum (not to be confused with the stellar continuum). The polynomial is fitted to the spectrum over the wavelength ranges 10.66–12.59 μm and 13.72–15.18 μm, and we define the 13 μm emission as the excess emission above the polynomial from 12.70 to 13.41 μm. We also use the polynomial to estimate the rms noise in the spectrum. To check the results, we fit both a fifth-degree and sixth-degree polynomial to each spectrum. A feature is detected if and only if (1) both polynomials give a 4 σ detection, and (2) in one of the two fits, the 13 μm emission is stronger than 5% of the continuum (as defined by the polynomial). This conservative approach will help guarantee the purity of our sample of 13 μm sources. Unfortunately, it will also select against fainter sources where the lower signal/noise levels might hide a 13 μm feature.

Table 2 presents results for our analysis of each aspect of our sample of spectra: averages and standard deviations for the

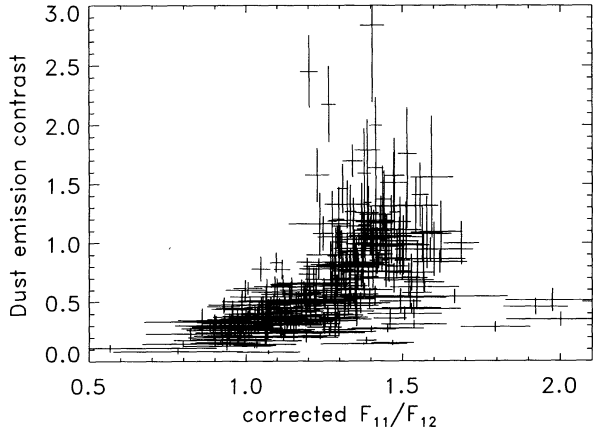


FIG. 4.—Dust emission contrast as a function of corrected flux ratio $F_{11}/F_{12}$. The error bars are as described for Fig. 2. The contrast is limited at each flux ratio, and this limit increases as the corrected flux ratio $F_{11}/F_{12}$ increases (i.e., as the emission profile grows narrower). Thus, high-contrast emission always has a narrow profile, but low-contrast emission can be narrow or broad.

corrected flux ratios $F_{11}/F_{12}$, dust emission contrast, [12]–[25] color, and fraction of 13 μm sources for each silicate emission class (abbreviated SE class). Throughout this paper, $[12]-[25] = 2.5 \log (F_{25}/F_{12}) + 1.56$.

In this paper, we will limit our discussion of the 13 μm feature to how it effects the classification of the silicate emission profile. A more complete discussion of the 13 μm emission and the kinds of sources which produce it is provided by Sloan, LeVan, & Little-Marenin (1995).

## 3. COMPARISON WITH EXISTING CLASSIFICATION SCHEMES

### 3.1. *LML Classes*

Little-Marenin & Little (1990) classified the dust emission profiles in 291 oxygen-rich Mira variables. Figure 5 shows how the LML classes of the 198 sources in common with our study are distributed along our silicate dust sequence. Because Little-Marenin and Little did not use the flux ratios to distinguish between classes, we expect some blurring of their classes, which does occur. Table 3 provides averages and standard deviations of the corrected $F_{11}/F_{12}$, dust emission contrast, and [12]–[25] color for each of their classes.

The overlap of the 3-component and Silicate++ classes is substantial, suggesting that they may not be separate classes. We have already noted that the 13 μm feature, used by Little-

TABLE 2

PROPERTIES OF THE SILICATE EMISSION CLASSES

| Class | Total | Corrected $F_{11}/F_{12}$ | Dust Emission Contrast | [12]–[25] | Fraction of 13 μm Sources |
|---|---|---|---|---|---|
| N[a] ..... | 84 | 0.92 ± 1.01 | −0.01 ± 0.03 | 0.09 ± 0.09 | 0.04 |
| SE1 ..... | 59 | 0.87 ± 0.09 | 0.21 ± 0.10 | 0.57 ± 0.16 | 0.36 |
| SE2 ..... | 69 | 1.00 ± 0.03 | 0.32 ± 0.14 | 0.64 ± 0.15 | 0.25 |
| SE3 ..... | 81 | 1.10 ± 0.03 | 0.37 ± 0.16 | 0.72 ± 0.15 | 0.32 |
| SE4 ..... | 55 | 1.20 ± 0.03 | 0.52 ± 0.37 | 0.79 ± 0.19 | 0.31 |
| SE5 ..... | 68 | 1.30 ± 0.03 | 0.68 ± 0.38 | 0.90 ± 0.22 | 0.26 |
| SE6 ..... | 69 | 1.39 ± 0.03 | 0.92 ± 0.45 | 0.88 ± 0.22 | 0.20 |
| SE7 ..... | 31 | 1.50 ± 0.03 | 0.84 ± 0.40 | 0.80 ± 0.20 | 0.23 |
| SE8 ..... | 21 | 1.71 ± 0.19 | 0.73 ± 0.39 | 0.91 ± 0.25 | 0.29 |

[a] Class N = naked star.

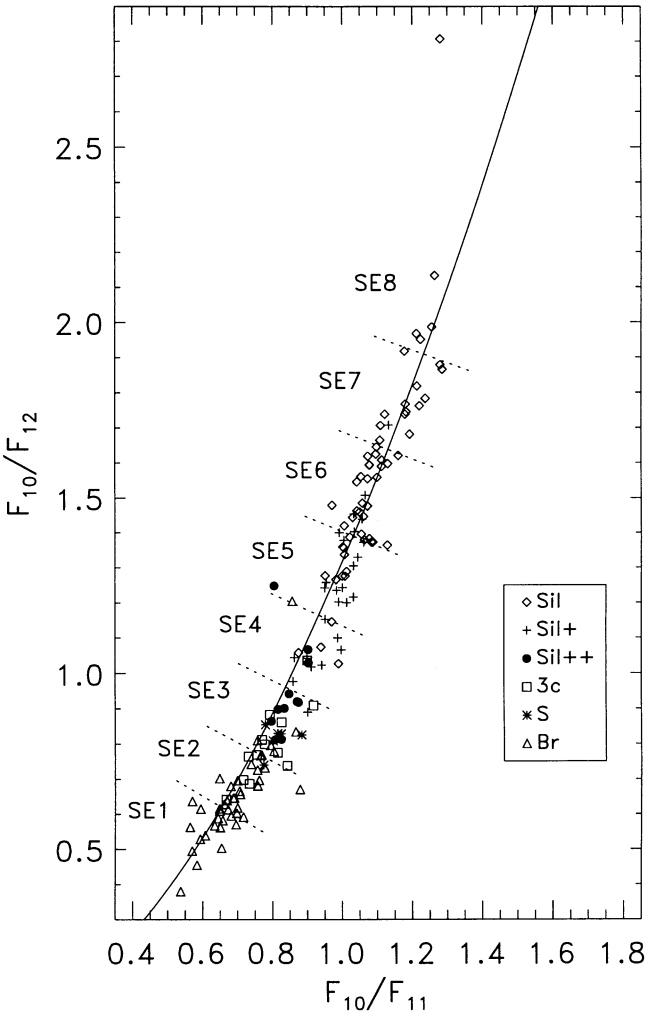


FIG. 5.—The location of the LML classes on the silicate dust sequence, based on the sample of Mira variables studied both here and by Little-Marenin & Little (1990). The solid line is the same power law in Fig. 2. Some overlap between the different LML classes is expected, since they used different criteria to make their classifications. However, the overlap between the 3-component, S, and Silicate++ classes is particularly large, suggesting that they may not be separate classes.

Marenin and Little as the defining characteristic of the 3-component class, occurs in other classes as well, as shown in Table 3. We conclude that the 3-component class, as defined in the LML system, is not a distinct class.

Little-Marenin & Little (1988) investigated the LRS spectra of a large number of MS and S stars and suggested that the unusual chemistry in the dust (caused by a C/O ratio near unity or by some of the rare *s*-process elements dredged up in the envelopes of these stars) might produce unusual dust excesses. They created a separate class of silicate emission, the S class, which they associated with S stars and described as having peak emission at 10.5–10.8 $\mu$m. However, a recent analysis of the LRS spectra of S stars by Chen & Kwok (1993) concluded that the infrared spectra of S stars exhibited no significant differences from oxygen-rich photospheres. We find that the distribution of S class dust emission along the silicate dust sequence completely overlaps the Silicate++ and 3-component classes, calling into question its existence as a separate class in the LML system.

TABLE 3

PROPERTIES OF THE LML CLASSES

| Class | Total | Corrected $F_{11}/F_{12}$ | Dust Emission Contrast | [12]–[25] | Fraction of 13 $\mu$m Sources |
|---|---|---|---|---|---|
| N ..... | 4 | 0.78 ± 0.53 | 0.14 ± 0.05 | 0.51 ± 0.06 | 0.00 |
| Br ..... | 54 | 0.97 ± 0.08 | 0.30 ± 0.10 | 0.57 ± 0.12 | 0.17 |
| S ..... | 11 | 1.04 ± 0.17 | 0.39 ± 0.13 | 0.68 ± 0.13 | 0.18 |
| 3C ..... | 17 | 1.08 ± 0.06 | 0.41 ± 0.14 | 0.64 ± 0.11 | 0.06 |
| Silicate++... | 15 | 1.15 ± 0.05 | 0.50 ± 0.09 | 0.73 ± 0.12 | 0.27 |
| Silicate+ ..... | 31 | 1.29 ± 0.08 | 0.73 ± 0.24 | 0.81 ± 0.19 | 0.16 |
| Silicate ..... | 66 | 1.42 ± 0.11 | 0.94 ± 0.30 | 0.87 ± 0.21 | 0.08 |

However, we should emphasize that our classification method does not examine a spectrum in the same detail as the LML system. The defining characteristic of the S class in the LML system is that the dust emission peaks from 10.5 to 10.8 $\mu$m. Because our system examines the flux at three discrete wavelengths (10.0, 11.0, and 12.0 $\mu$m), it cannot distinguish details such as this. While we have reason to question the nature of the S class, our system cannot rule out its existence.

Because the defining characteristic of the 3-component class is the 13 $\mu$m feature (in addition to features at 10 and 11 $\mu$m) and we do examine the 13 $\mu$m feature, our conclusions about this class are a little stronger. At the very least, this class is misnamed in the LML system. Little-Marenin & Little (1994) emphasize that there are other aspects of the typical 3-component spectrum, such as a sharp rise in emission on the short-wavelength side of the 10 $\mu$m feature, which our classification does not address.

### 3.2. *Low-Resolution Spectrometer Characterizations*

The LRS characterizations are based primarily on the contrast of the shell, as shown in Table 4. The dust emission contrast increases steadily and monotonically from LRS characterization 21 to 29, although there is a substantial spread of contrast for each characterization. This spread results from the decision of the *IRAS* Science Team to fit a continuum to the flux at 13.3 $\mu$m when determining the LRS characterization, based on the erroneous assumption that there is no dust contribution at that wavelength.

TABLE 4

PROPERTIES OF THE LOW-RESOLUTION SPECTROMETER CHARACTERIZATIONS

| Class | Total[a] | Corrected $F_{11}/F_{12}$ | Dust Emission Contrast | [12]–[25] | Fraction of 13 $\mu$m Sources |
|---|---|---|---|---|---|
| 18..... | 52 | 1.03 ± 0.99 | −0.02 ± 0.02 | 0.06 ± 0.07 | 0.00 |
| 17..... | 31 | 0.68 ± 0.50 | 0.04 ± 0.04 | 0.26 ± 0.20 | 0.13 |
| 16..... | 39 | 0.94 ± 0.22 | 0.15 ± 0.04 | 0.54 ± 0.17 | 0.23 |
| 15..... | 73 | 0.99 ± 0.08 | 0.27 ± 0.05 | 0.62 ± 0.13 | 0.34 |
| 14..... | 20 | 0.97 ± 0.10 | 0.38 ± 0.06 | 0.68 ± 0.15 | 0.50 |
| 21..... | 17 | 1.11 ± 0.08 | 0.35 ± 0.10 | 0.72 ± 0.13 | 0.41 |
| 22..... | 52 | 1.18 ± 0.09 | 0.41 ± 0.15 | 0.76 ± 0.15 | 0.35 |
| 23..... | 38 | 1.25 ± 0.10 | 0.48 ± 0.12 | 0.82 ± 0.17 | 0.29 |
| 24..... | 30 | 1.34 ± 0.09 | 0.58 ± 0.10 | 0.82 ± 0.14 | 0.37 |
| 25..... | 17 | 1.44 ± 0.21 | 0.71 ± 0.19 | 0.83 ± 0.17 | 0.29 |
| 26..... | 29 | 1.40 ± 0.14 | 0.80 ± 0.16 | 0.91 ± 0.17 | 0.28 |
| 27..... | 16 | 1.41 ± 0.08 | 0.95 ± 0.20 | 0.87 ± 0.24 | 0.13 |
| 28..... | 28 | 1.43 ± 0.09 | 1.09 ± 0.19 | 0.95 ± 0.26 | 0.11 |
| 29..... | 27 | 1.46 ± 0.09 | 1.44 ± 0.40 | 1.01 ± 0.18 | 0.19 |

[a] Not included are 18 sources with other LRS characterizations and 50 sources with no LRS characterization.

TABLE 5

PROPERTIES OF THE AUTOCLASSES

| Class | Total[a] | Corrected $F_{11}/F_{12}$ | Dust Emission Contrast | [12]–[25] | Fraction of 13 μm Sources |
|---|---|---|---|---|---|
| δ0 ..... | 69 | 0.92 ± 0.92 | −0.01 ± 0.03 | 0.09 ± 0.09 | 0.03 |
| λ25 ..... | 54 | 1.05 ± 0.30 | 0.15 ± 0.06 | 0.52 ± 0.17 | 0.13 |
| λ30 ..... | 113 | 1.01 ± 0.10 | 0.29 ± 0.08 | 0.64 ± 0.12 | 0.32 |
| λ34 ..... | 49 | 1.12 ± 0.08 | 0.55 ± 0.11 | 0.83 ± 0.14 | 0.53 |
| β8 ..... | 72 | 1.32 ± 0.09 | 0.59 ± 0.17 | 0.82 ± 0.14 | 0.36 |
| β11 ..... | 10 | 1.31 ± 0.08 | 1.66 ± 0.59 | 1.17 ± 0.17 | 0.30 |
| β0 ..... | 30 | 1.37 ± 0.06 | 1.04 ± 0.23 | 1.07 ± 0.18 | 0.10 |
| β1 ..... | 47 | 1.47 ± 0.08 | 1.07 ± 0.24 | 0.86 ± 0.19 | 0.21 |
| λ12 ..... | 14 | 1.61 ± 0.24 | 0.37 ± 0.11 | 0.84 ± 0.14 | 0.14 |

[a] Not included are 29 sources with other autoclasses and 50 sources with no autoclass.

The LRS 1*n* characterizations remain misunderstood in the literature. As can be seen from Table 4, only spectra of LRS characterization 18 truly contain no dust emission, i.e., represent naked stars. Excess emission is present in some LRS characterization 17 sources and increases monotonically from 17 to 14. This fact can also be seen from the average [12]–[25] colors for each LRS characterization. The definition of the 1*n* subclasses provides another argument. For example, a spectrum with a characterization of 16 can be modeled with a smooth continuum where $F_\lambda \propto \lambda^3$. If this emission arose from the star alone, the effective temperature would only be about 900 K, far too low to be physically valid. A more reasonable interpretation is that the spectrum contains a stellar contribution and a weak excess, as pointed out by Little-Marenin & Little (1988) and others. Despite this fact, the practice continues of describing all sources with 1*n* LRS characterizations as naked stars with no excesses.

Additionally, we note that LRS characterizations 14 and 21 overlap. While they both have about the same emission contrast, the characterization algorithm appears to have labeled narrower features as 21 and broader ones as 14, as can be seen from the corrected flux ratios $F_{11}/F_{12}$ in Table 4.

Finally, we find that sources with low-contrast emission present problems for the LRS characterizations. Low contrast usually leads to a poor signal-to-noise ratio for the emission component, and this frequently results in misclassifications. It is not unusual to find low-contrast silicate emission classed as 41 (weak SiC emission) or 31 (weak silicate absorption). Our sample of 537 emission spectra from oxygen-rich dust includes nine spectra with LRS characterizations of 41 and three characterized as 42 or 43.

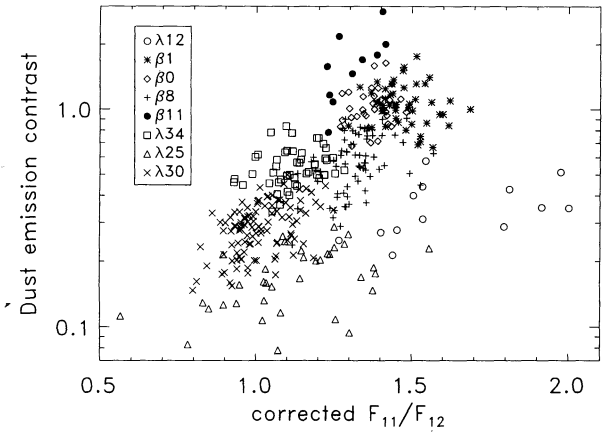


FIG. 6.—Plotting dust emission contrast vs. corrected $F_{11}/F_{12}$ illustrates how the autoclass algorithm of Cheeseman et al. (1989) divided the many apparent silicate emission spectra into different groups. Each autoclass occupies a different region on this plot, with only some overlap between adjacent autoclasses.

### 3.3. *Autoclasses*

Because the autoclass algorithm used the total appearance of a spectrum to determine its class, all three characteristics we have tried to separate here, dust emission contrast, shape of the dust emission spectrum, and 13 μm emission, contribute to the final classification. While this fact has made it difficult to relate the autoclasses to observed parameters and other classification systems, the autoclasses have proven extremely useful by pointing out natural groupings of spectra within the extensive LRS database.

Table 5 gives the results of our analysis. Most of the 537 variables in our sample fall into nine autoclasses. We conclude that for spectra with oxygen-rich dust emission, the autoclasses were separated primarily on the basis of two variables: dust emission contrast and shape of the emission profile. This dependency is illustrated in Figure 6.

Autoclasses λ12 and β1 correspond to silicate emission indices of 7–8 and 6–7 respectively. Based on the flux ratios, autoclasses β0, β8, and β11 all correspond roughly to silicate indices 4–6; the major difference between these groups, as illustrated in Figure 6, is their dust emission contrasts. As a group, autoclasses λ34 and λ30 correspond to the broader emission profiles, indices 1–4; again, the primary distinction between them is their dust emission contrast. Autoclass λ25 represents the lowest contrast shells, with a mean contrast of only 15%, with little or no consideration of the shape of the emission. Finally, autoclass δ0 represents the same group of stars as our N class (no emission).

The descriptions of each autoclass by Cheeseman et al. (1989) suggested that 13 μm emission appeared in most members of classes β8, λ34, λ25, λ30, and perhaps among some members of β11. Our analysis confirms this result for all of these classes except λ25. The relatively low percentage of 13 μm sources among the members of autoclass λ25 is probably an artifact of our method, which tends to select against the lowest contrast shells. Cheeseman et al. (1989) did not mention 13 μm emission in the autoclasses λ12, β0, and β1, but our analysis reveals 13 μm emission in 10%–20% of these sources as well. The high percentage of 13 μm emission sources among autoclass λ34 is striking. The autoclass algorithm may have used the shape of the spectrum at 13 μm as a secondary constraint on membership in this class and may have adjusted the class boundaries to include as many 13 μm sources as possible.

## 4. DISCUSSION

### 4.1. *Emission Features Related to Silicate Dust*

We can identify a minimum of four dust components in our sample of oxygen-rich AGB variables. The classic silicate feature at 10 μm is the best understood of these (e.g., Ossenkopf et al. 1992); it is produced by amorphous silicates. Several authors have suggested that spectra containing emission components at 10 and 11 μm (SE4–6 or Silicate+ and Silicate++) arise from crystalline olivine (Tielens 1989; Little-Marenin & Little 1990; Nuth & Hecht 1990). The broad emission component (SE1–3) has been associated with alumina grains

(Vardya, deJong, & Willems 1986; Onaka, deJong, & Willems 1989), but the specific identification with $\gamma$-$Al_2O_3$ does not provide an ideal match with the data (Tielens 1989). The origin of the 13 $\mu$m feature is very debatable. Corundrum ($\alpha$-$Al_2O_3$, a crystalline structure) could account for the feature (Glaccum 1994), but evidence to support this hypothesis has not yet been published. While the carrier of the 13 $\mu$m feature is probably an oxide (Tielens 1989), it is difficult to say much more with confidence.

### 4.2. *The Silicate Dust Sequence*

Stencel et al. (1990) have argued that the sequence from broad to narrow silicate emission is both a chemical and evolutionary sequence, based on the association of the broad emission feature with alumina and the correlation of the sequence from broad to narrow emission with the evolutionary maser sequence of Lewis (1989). In this scenario, grains form first from condensing alumina material. Then, as the grains evolve, silicate material begins to dominate the emission. Fresh silicate material would be crystalline and exhibit emission components at 10 and 11 $\mu$m, while grains in more extended shells would be amorphous and exhibit the classic silicate feature.

Egan & Sloan (1995) point out that the silicate dust sequence can be reproduced by increasing the optical depth of the circumstellar dust shell until it exhibits self-absorption at 10 $\mu$m. If this were an evolutionary scenario, the youngest shells would have the narrowest features. Older shells would be thicker, and self-absorption of the silicate emission would broaden the 10 $\mu$m feature. We would then expect that broad emission features would be associated with very red [12]–[25] colors. As can be seen from Tables 2 and 3, the broad emission features tend to arise from a bluer population, ruling out the possibility that the entire silicate dust sequence results from self-absorption of the silicate feature.

It is still possible that *some* of our sample do show self-absorption. In Table 2, the [12]–[25] color increases steadily from SE1 to SE4 but remains roughly constant from SE5 to SE8. The standard deviations are larger for these sources also, suggesting that two types of sources may be contained in these classes: optically thin shells with emission components at 10 and 11 $\mu$m and thicker shells showing slight self-absorption. Recall that we rejected the three reddest Mira variables from our sample because they clearly exhibited self-absorbed silicate emission. We suspect that a fraction of our sources, especially around SE5 and SE6, may have self-absorbed emission.

### 4.3. *Silicate Emission Indices and Dust Shell Evolution*

To examine what the silicate dust sequence can tell us about the evolution of circumstellar dust shells, we adopt the following simple scenario. First, we assume that grains evolve as described by Stencel et al. (1990). Second, we assume that stars produce one shell which evolves from geometrically and optically thin to thick, causing the observed star to evolve from a visual AGB to OH/IR star. Finally, we assume that the variability class of stars evolves in the sequence Lb–SRb–SRa–Mira.

If all three assumptions are valid, then we expect that as we move along the variability sequence from irregular to Mira, we will see a decreasing proportion of broad spectra (SE1–3) and an increasing proportion of narrow spectra (SE7–8). Figure 7 demonstrates that this does not happen, so one or more of our assumptions must be incorrect.

A recent study of oxygen-rich semiregular and irregular variables by Jura & Kleinmann (1992) concluded that while all

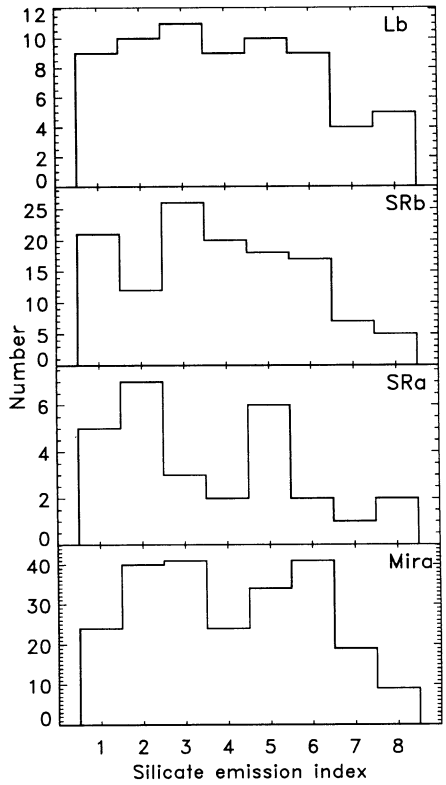


FIG. 7.—The distribution of silicate emission indices for each variability class in our sample. There are some differences in the distributions, but no systematic trends are apparent. If irregular variables were more likely to have young circumstellar shells and Mira variables more evolved shells, and if these shells followed the evolutionary scenario of Stencel et al. (1990), then the broad emission indices (SE1-3) should be concentrated in the irregular variables, and narrow emission indices (SE6-8) should be concentrated in the Mira variables.

Mira variables pulsate in the fundamental mode, many of the semiregular variables, particularly those with periods less than 150 days, pulsate in the first (or even second) overtone mode. Their study and a study of semiregular variables by Kerschbaum & Hron (1992) suggest that as stars evolve up the AGB, they evolve from irregular to semiregular to Mira variables as pulsational instabilities develop, settle into the fundamental mode, and grow in amplitude. The mass-loss rates derived by Jura & Kleinmann (1992) increase from $\sim 10^{-8}\ M_\odot\ \mathrm{yr}^{-1}$ for irregular and overtone semiregular variables to $\sim 10^{-7}\ M_\odot\ \mathrm{yr}^{-1}$ for fundamental pulsators. This result is fully consistent with how the percentage of stars surrounded by dust increases along the sequence from irregular to Mira variables (see Table 1). Only 67% of the irregulars have circumstellar dust. This fraction increases to 80% of the SRb variables, 97% of the SRa variables, and 99% of the Mira variables. We believe that the variability sequence is valid, at least in a statistical sense. Kerschbaum & Hron (1992) suggest that thermal pulsing on the AGB probably upsets the pulsation mode of a star and could cause a Mira to revert briefly to a semiregular or even an irregular variable, thus upsetting the sequence for a small fraction of the sources at a given time.

Examining how the mean spectral class changes with silicate emission index provides a similar test. This test replaces the assumption that stars evolve from irregular to Mira variables with the assumption that more evolved stars will be further up the AGB and of later spectral class. Again, the result is the

same (see Fig. 8). While stars with no dust emission (naked stars) are associated with earlier spectral classes, among the silicate emission indices there is virtually no difference in the distribution of spectral classes.

The evolutionary scheme for dust shells proposed by Stencel et al. (1990) is compelling, but Tielens (1989) argues that the chemistry of forming grains will depend crucially on the physical conditions of the dust formation region. The relation between the asymmetry of the optical light curve and the spectral emission from the dust (first discussed by Vardya et al. 1986) could indicate that the type of dust formed depends on how the shocks passing through the Mira atmosphere interact with the dust formation zone (Tielens 1995).

Observations of multiple-shell structure in two bright evolved stars call into question the assumption that AGB sources only produce one shell. Sloan, Grasdalen, & LeVan (1993), using a mid-infrared long-slit spectrometer, and Danchi et al. (1994), using a mid-infrared spatial interferometer, showed that the supergiant $\alpha$ Orionis is enclosed within two optically thin dust shells, suggesting that the mass-loss rate from this source varies with time. IRC +10216, an extreme carbon star and long-period Mira variable, also shows multiple shells (e.g., Sloan & Egan 1995). Both IRC +10216 and $\alpha$ Orionis are among the 10 brightest stars in the mid-infrared sky, leading us to suspect that multiple shells around evolved stars may be the rule and not the exception. It is possible that during each episode of enhanced mass loss, a new interior shell forms, evolving chemically as suggested by Stencel et al. (1990).

### 4.4. *Possible Applications of This Classification Method*

This study does not address how the spectrum from the dust shell changes with phase of the central star. For brighter sources, individual LRS scans can be examined to probe this issue, as Little-Marenin, Stencel, & Staley (1995) have done for AU Cygni. We have also examined individual LRS scans for a small number of bright Mira variables and find that changes in the silicate emission index tend to be small.

For most Mira variables observed by the LRS, multiple scans are available, but, in general, the full period of the variable is not covered adequately to search for variations in the spectral shape. Another approach would be to monitor a selected group of variables from the ground with sufficient time resolution to completely cover the period of variability. If the monitoring were done with a spectrometer, the classification method introduced here could be applied to the data to search for subtle variations in the shape of the emission.

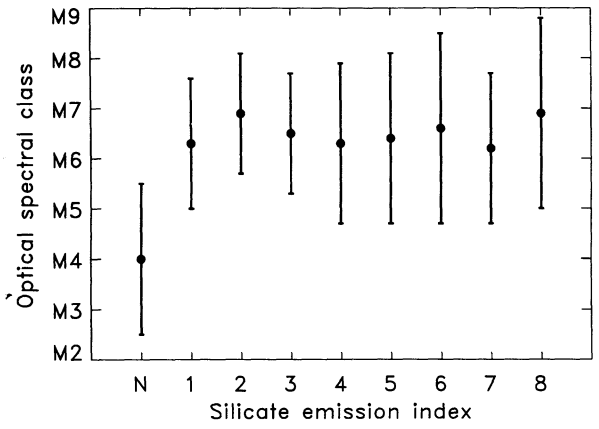


FIG. 8.—The lack of correlation of silicate emission index with optical spectral class, illustrated here by plotting the mean optical spectral class and standard deviation for each silicate emission index. While all the silicate emission indices show approximately the same distribution of spectral classes, the naked stars represent a distribution of earlier type stars.

This classification method could also be modified for narrow-band photometry. A minimum of three filters would be needed, one to isolate the stellar contribution at 7–9 $\mu$m and at least two covering the silicate emission feature from 10 to 12 $\mu$m. Many infrared photometric systems meet these criteria, although for most, the short-wavelength filter is generally centered at 8.4–8.7 $\mu$m wavelengths where the silicate emission begins to contribute to the flux, especially for high-contrast shells. For some systems, the third filter is centered beyond 12.0 $\mu$m, too red to be very useful. An ideal system would have three filters centered at 8.2, 10.5, and 11.5 $\mu$m, or four filters centered at 8.2, 10.0, 11.0, and 12.0 $\mu$m. The bandpasses in an ideal system would be narrower than the 0.8–1.2 $\mu$m bandpasses typical for most infrared filter systems.

## 5. SUMMARY

1. We have discovered that the observed profile of the silicate dust emission at 10 $\mu$m is constrained to a narrow sequence of shapes from broad to narrow emission. This silicate dust sequence provides a straightforward means of classifying emission from silicate dust and validates the sequence of silicate emission classes first proposed by Little-Marenin & Little (1988, 1990).

2. An examination of the 13 $\mu$m emission feature calls into question the 3-component class of Little-Marenin and Little and shows that the 13 $\mu$m feature occurs in a wide range of silicate emission profiles.

3. Our method does not distinguish the S class of Little-Marenin and Little as a separate class of emission from oxygen-rich dust.

4. A comparison of our classifications to the LRS characterizations of silicate emission spectra reveals that the LRS characterizations are based on contrast, although their contrast measurements are of limited value. Furthermore, we emphasize that sources with LRS characterizations of 14–17 are not naked stars, but contain excess emission.

5. An examination of the autoclasses (Cheeseman et al. 1989) shows that this algorithm distinguished silicate emission spectra primarily on the basis of contrast and silicate emission shape. The 13 $\mu$m feature appears to be a minor discriminant.

6. There are no tendencies of any silicate emission shape to be associated particularly with any variability class or optical spectral class, calling into question the evolutionary sequence for dust shells proposed by Stencel et al. (1990) or suggesting that as stars evolve up the AGB, they undergo episodic mass loss and produce multiple shells.

We gratefully acknowledge useful and stimulating discussions with R. E. Stencel, I. R. Little-Marenin, H. M. Dyke, J. Goebel, and A. G. G. M. Tielens. The comments and suggestions of S. Little, the referee, resulted in many improvements to this paper. The authors have used the LRS databases maintained at the University of Calgary and the University of Colorado, Boulder, the SIMBAD database in Strasbourg, and data distributed by NASA's Astronomical Data Center. The FITS Table Browser software written by L. Brotzman has been most helpful. G. C. S. received support from the Phillips Lab Scholar program and the National Research Council.

REFERENCES

Beichman, C. A., Neugebauer, G., Habing, H. J., Clegg, P. E., & Chester, T. J., ed. 1988, *IRAS* Catalogs and Atlases: Explanatory Supplement (Washington: GPO)
Cheeseman, P., Stutz, J., Self, M., Taylor, W., Goebel, J., Volk, K., & Walker, H. 1989, Automatic Classification of Spectra from the *Infrared Astronomical Satellite* (*IRAS*) (NASA RP-1217) (Washington: GPO)
Chen, P. S., & Kwok, S. 1993, ApJ, 416, 769
Cohen, M., Walker, R. G., & Witteborn, F. C. 1992, AJ, 104, 2030
Danchi, W. C., Bester, M., Degiacomi, C. G., Greenhill, L. J., & Townes, C. H. 1994, AJ, 107, 1469
Draine, B. T., & Lee, H. M. 1984, ApJ, 285, 89
Egan, M. P., & Sloan, G. C. 1995, in preparation
Engelke, C. W. 1992, AJ, 104, 1248
Glaccum, W. 1995, in Proc. of the Airborne Astronomy Symp. on the Galactic Ecosystem: From Gas to Stars to Dust, ed. M. R. Haas, J. A. Davidson, & E. F. Erickson (San Francisco: ASP), 395
Goebel, J., Volk, K., Walker, H., Gerbault, F., Cheeseman, P., Self, M., Stutz, J., & Taylor, W. 1989, A&A, 222, L5
Hoffmeister, C., Richter, G., & Wenzel, W. 1984, Variable Stars (Berlin: Springer)
*IRAS* Point Source Catalog, Version 2.0. 1988, Joint *IRAS*, Science Working Group (Washington: GPO) (PSC)
*IRAS* Science Team. 1986, A&AS, 65, 607 (LRS Atlas)
Jura, M., & Kleinmann, S. G. 1992, ApJS, 83, 329
Kerschbaum F., & Hron, J. 1992, A&A, 263, 97
Kholopov, P. N., et al. 1985–1988, General Catalogue of Variable Stars (4th ed.; Moscow: Nauka, & Greenbelt: NASA Astronomical Data Center) (GCVS)
Lang, K. R. 1992, Astrophysical Data: Planets and Stars (New York: Springer)
Lewis, B. M. 1989, ApJ, 328, 234
Little-Marenin, I. R., & Little, S. J. 1988, ApJ, 333, 305
———. 1990, AJ, 99, 1173
———. 1994, private communication
Little-Marenin, I. R., & Price, S. D. 1986, in Summer School on Interstellar Processes: Abstracts of Contributed Papers, ed. D. J. Hollenbach & H. A. Thronson NASA Tech. Memo. 88342, 137
Little-Marenin, I. R., Stencel, R. E., & Staley, S. B. 1995, in preparation
Nuth, J. A., & Hecht, J. H. 1990, Ap&SS, 163, 79
Onaka, T., DeJong, T., & Willems, F. 1989, A&A, 218, 169
Ossenkopf, V., Henning, T., & Mathis, J. S. 1992, A&A, 261, 567
Rinsland, C. P., & Wing, R. F. 1982, ApJ, 262, 212
Sloan G. C., & Egan, M. P. 1995, ApJ, 444, in press
Sloan, G. C., Grasdalen, G. L., & LeVan, P. D. 1993, ApJ, 404, 328
Sloan, G. C., LeVan, P. D., & Little-Marenin, I. R. 1995, in preparation
Stencel, R. E., Nuth, J. A., Little-Marenin, I. R., & Little, S. J. 1990, ApJ, 350, L45
Tielens, A. G. G. M. 1989, From Miras to Planetary Nebulae: Which Path for Stellar Evolution?, ed. M. O. Mennessier & A. Omont (Gif-sur-Yvette: Editions Frontières), 186
———. 1995, private communication
Vardya, M., deJong, T., & Willems, F. 1986, ApJ, 304, L29
Volk, K., & Cohen, M. 1989, AJ, 98, 931
Wildeman, K. J., Beintema, D. A., & Wesselius, P. R. 1983, J. Brit. Interplanetary Soc., 36, 21